Thermally induced chemical evolution in polyimide films investigated by X-ray photoelectron spectroscopy

Battirola, Liliane C.; Rudolf, Petra; Tremiliosi-Filho, Germano; Rodrigues-Filho, Ubirajara P.

Published in:
Polymer Engineering and Science

DOI:
10.1002/pen.24649

Thermally Induced Chemical Evolution in Polyimide Films Investigated by X-ray Photoelectron Spectroscopy

Liliane C. Battirola,[1] Petra Rudolf,[2] Germano Tremiliosi-Filho,[1] Ubirajara P. Rodrigues-Filho[1]
[1] *Chemistry Institute of São Carlos, Department of Chemical Physics, University of São Paulo, São Carlos, 13563-120, Brazil*
[2] *Zernike Institute for Advanced Materials, Department of Physics, University of Groningen, Nijenborgh 4, Groningen, AG, 9747, The Netherlands*

Thermally modified polyimide films based on 1,4-Phenylene diamine (p-PDA) and 3,3′,4,4′ – Benzophenone tetracarboxylic dianhydride (BTDA) were prepared and their chemical structure transformation after thermal treatment at 350 °C–500 °C was investigated. X-ray diffraction results revealed an increase in the polymer chain order for all treated PI samples as a consequence of the thermal treatment and chain interaction. TGA analysis showed that the heat treatment promoted different thermal degradation profiles. Electron spin resonance evidenced a large population of free radicals as a result of homogeneous bond cleavage when the thermal treatment was performed at 500 °C. X-ray photoelectron spectroscopy analysis indicated that the chemical structure transformation not only occurs on the outer surface but also in the sub-surface layer. These results show that controlled fast thermal treatment can produce materials with specific characteristics and may serve as a general strategy for changing both structural and chemical properties of the polymers.
POLYM. ENG. SCI., 58:943–951, 2018.

INTRODUCTION

Polyimides (PI) are versatile polymers as they are obtained by polycondensation reactions where it is possible to tailor their physico-chemical properties through the choice of the monomers used. The imide moiety with its aromatic backbone confers to the polymer enhanced mechanical strength, chemical resistance, optical properties, and thermal stability [1–4]. There are reports of obtaining chemically and/or physically modified PI polymers for use in gas separation or water filtration. For example, some improvements in selective transport of small molecules and ions have been made by modifying the cavity structure in PI-based membranes [5, 6]. There are also studies using structurally modified PI polymers as insulator [7] or conductor (electrolyte) materials [8–11].

Among the many methods reported for improving some specified propriety of these PIs [12–15], thermal treatment seems to be a promising direction for building materials with tuneable porous structures besides allowing for easy up scaling. For example, there have been independent reports of PI modification obtained using a post-synthesis step of thermal treatment either under an oxidizing (O_2 or air) [16] or an inert (vacuum, nitrogen, or argon) atmosphere [17, 18]. Specifically, the thermal treatment should not result in loss of mechanical strength, thermal, and chemical stability, which would significantly compromise PI's potential for application. Thermal treatments under oxidizing atmosphere showed to be trickier to control and may not be applicable in many cases. Conversely, thermal processing under inert conditions using precisely controlled thermal cycles may induce variations in the polymer morphology and structure. In fact, thermal treatment can induce electron-rich aromatic rings to get closer to electron-deficient rings under the influence of intramolecular and intermolecular forces, leading to the formation of both more dense chain packing and carbonized surface layers depend on the used temperature [12, 19]. A heat treatment at medium temperatures has revealed better selectivity in terms of gas permeability for use as separation membranes, owing to the densely packed structures [20]. Treatments at higher temperatures (500 °C–900 °C) however, produce the growth of carbon structures in the film via a thermolysis reaction, which can affect directly the chemical selectivity of the PI when used as molecular sieves [18, 21]. The thermolysis takes place from the surface inwards and may result in an aromatic carbon structure, which changes the chemical interaction with molecules passing through the membrane. Although much progress has been made in the fabrication of PI films by thermal treatments under inert condition, many questions concerning the factors governing the formation of densely packed structures and/or carbon layers remain unanswered [22–24].

Herein we report insights into the evolution of the thermally induced structural transformation in poly(imide) films by X-ray photoelectron spectroscopy (XPS)—a selective surface analysis technique. We used different photon energies and thereby varied the inelastic mean free path of the photoelectrons to investigate the chemical evolution of the films as function of temperature (350 °C to 500 °C) from the surface inwards, *i.e.*, in a temperature range that enables its physical or chemical modification. Further characterization with infrared spectroscopy, electron spin resonance (ESR), and X-ray diffraction (XRD) was carried out to gain a deeper understanding.

EXPERIMENTAL

Chemicals

1,4-Phenylene diamine 97% (p-PDA) and 3,3′,4,4′ – Benzophenone tetracarboxylic dianhydride 96% (BTDA) were purchased from Sigma-Aldrich and used without prior purification;

Correspondence to: U. P. Rodrigues-Filho; e-mail: uprf@iqsc.usp.br
Contract grant sponsor: National Council of Technological and Scientific Development; contract grant number: CNPq-Brazil #5321-09-3; contract grant sponsor: European Community's Seventh Framework Programme; contract grant numbers: FP7/2007-2013; #226716; contract grant sponsor: São Paulo Research Foundation (FAPESP).
DOI 10.1002/pen.24649
Published online in Wiley Online Library (wileyonlinelibrary.com).

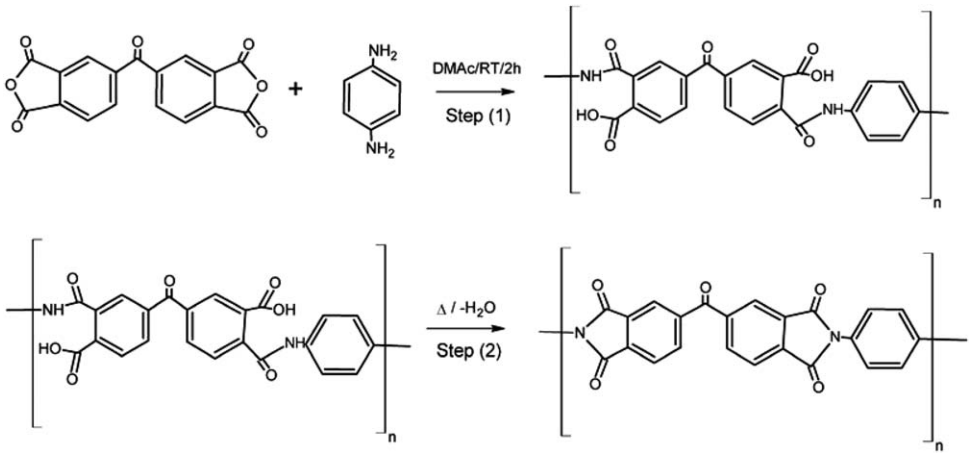

FIG. 1. Scheme of the synthesis steps of pre-polymer formation (1) and thermal polymerization (2) in the Polyimide preparation.

Dimethylacetamide 99% (DMAc) was purchased from Synth and was treated overnight with molecular sieves with 3 Å pores.

Polymer Synthesis

Polyimides films were synthesized using a two steps thermal imidization method [25, 26]. BTDA (1.60 mmol) and p-PDA (1.60 mmol) were added in a 50 mL two neck flask containing 7 mL of DMAc. The mixture was magnetically stirred for 2 h at room temperature to generate a viscous polyamic acid (PAA) solution (10 wt%) (step 1). Afterwards, the PAA solution was diluted in a DMAc (5 mL) solution. All the PI precursors were spread on a home-made Teflon® mold, and subsequently pre-dried in an oven at 80 °C for 14 h to remove most of the solvent. The semi-dry PAA film was further heated as follows: 100 °C/30 min, 200 °C/30 min, and 300 °C/60 min, allowing for the PI formation; under an argon atmosphere (step 2). The steps (1) and (2) of the reaction mechanism are shown schematically in Fig. 1.

Thermal Treatment

Before starting the heating steps, a MAITEC ceramic tube furnace was purged with argon for 5 min; then the PI samples were placed into and thermally treated at 350 °C, 400 °C, and 500 °C for 15 min under an argon flow (10 mL min^{-1}). After the heat treatment, the samples were cooled naturally to room temperature under argon flow. PI films treated at 350 °C, 400 °C, and 500 °C are labelled as PI350, PI400, and PI500 in the following.

Characterization Techniques

Vibrational Spectroscopy. Fourier transform infrared (FTIR) spectra in the range between 400 and 4,000 cm^{-1} were acquired using a Bruker FTIR spectrometer, model IFS 66 v/s, equipped with a deuterated triglycine sulfate detector. The data were collected in attenuated total reflectance (FTIR-ATR) at room temperature by averaging over 100 scans with a spectral resolution of 4 cm^{-1}.

X-ray Diffraction. XRD experiments were performed using a Rigaku Ultima IV diffractometer, operating at 40 kV and 40 mA for Cu Kα radiation ($\lambda = 1.5418$ Å); patterns were collected in continuous mode at 0.3° min^{-1} in a 2θ range from 1.5° up to 40°.

Thermogravimetric Analysis. Thermogravimetric analysis (TGA) was carried out using a Perkin Elmer Thermal Analysis equipment under nitrogen flow (20 mL min^{-1}). PI samples (5 mg) were placed in an alumina sample holder and heated from room temperature up to 900 °C at a rate of 10 °C min^{-1}.

Electron Spin Resonance. ESR measurements were performed with a Bruker Elexsys E580 spectrometer. Samples were kept at 77 K; the amplitude modulation was 2 G, the frequency applied was 100 kHz and the microwave power 0.16 mW.

X-ray Photoelectron Spectroscopy. XPS data were collected using a Surface Science SSX-100 ESCA instrument equipped with a monochromatic Al Kα X-ray source ($h\nu = 1{,}486.6$ eV). The electron take-off angle with respect to the surface normal was 37° and the pressure in the measurement chamber was $5x10^{-10}$ mbar. Photoemission spectra were also collected using hard X-rays ($h\nu = 4{,}000$ eV) at the HIKE experimental station on the KMC-1 bending magnet beamline of the synchrotron radiation source BESSY in Berlin, Germany. This beamline delivers X-rays in the range 1.7–12 keV. The HIKE end station is equipped with a Gammadata Scienta R-4000 hemispherical electron energy analyzer modified for high transmission and kinetic energy resolution of photoelectrons with energies up to 10 keV, for further details see [27]; the pressure during the data acquisition was 1×10^{-6} mbar. The experimental resolution was set to 1.7–1.9 eV for the spectra collected with the laboratory source and to 1.0–1.1 eV for those collected with synchrotron light. XPS spectra were analyzed using the least-squares curve fitting program Winspec (LISE laboratory, University of Namur). Deconvolution of the spectra included a Shirley baseline subtraction and fitting with a minimum number of peaks consistent with the molecular structure of the surface, taking into account the experimental resolution. The profile of the peaks was taken as a convolution of Gaussian and Lorentzian functions. The component at 284.7 eV binding energy in the C1*s* line was used as reference for correcting the binding energy scale [28]. To compensate for charging, the sample was irradiated with electrons from a flood gun, which was regulated to deliver a flux of electrons with 0.5 and 100 eV of kinetic energy

 DOI 10.1002/pen

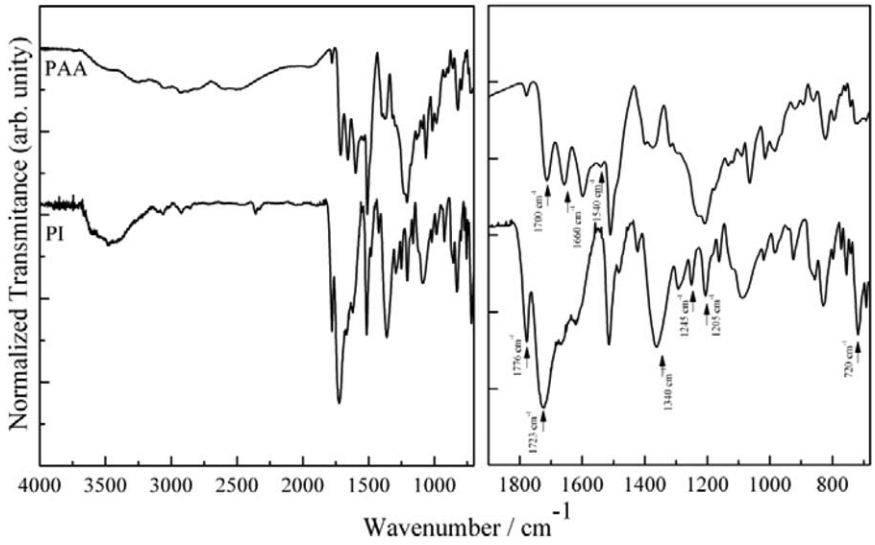

FIG. 2. FTIR-ATR spectra of the synthesized polyamic acid (PAA) precursor and of the polyimide film (PI) prior to thermal treatment. Arrows indicate the bands cited in the text.

for conventional and synchrotron XPS measurements, respectively [29].

RESULTS AND DISCUSSION

Prior to thermal treatment, the PAA precursor and synthesized PI film were characterized by FTIR-ATR spectroscopy. Figure 2 shows the FTIR–ATR spectra of both samples; a magnified view of the main bands is presented as well. The imidization synthesis involves the formation of imide rings, followed by the depletion of the amides groups (Fig. 1). Typical absorption bands related to the amide group at 3,320 cm^{-1} ($\upsilon_{N\text{-}H}$), 1,660 cm^{-1} ($\upsilon_{C=O}$), and 1,540 cm^{-1} ($\upsilon_{C\text{-}NH}$) as well as bands at 1,700 cm^{-1} ($\upsilon_{C=O}$) and 2,800–3,200 cm^{-1} (OH) related to the carboxylic acid groups were identified in the precursor material, confirming PAA formation. After the second synthesis step, absorption bands at 1,776 cm^{-1} ($\upsilon_{asC=O}$), 1,723 cm^{-1} ($\upsilon_{asC=O}$), 1,340 cm^{-1} ($\upsilon_{C–N–C}$ axial stretch), 1,205 cm^{-1} and 1,245 cm^{-1} ($\upsilon_{C–N–C}$ stretch), and 720 cm^{-1} ($\upsilon_{C–N–C}$ out-of-plane bending related to PI groups) were detected, indicating the formation of PI [30–32]. Conversely, bands related to the amide group disappeared, pointing to the conversion of PAA to PI. Peaks related to PI can also be observed in the PAA FTIR spectrum, which indicates that the imidization process started during the drying step.

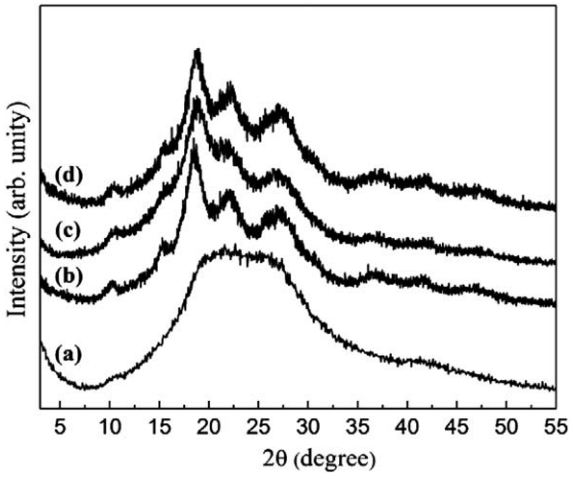

FIG. 3. XRD diffractograms of (a) the synthesized polyimide film before (PI), and after heat treatment at (b) 350 °C (PI350), (c) 400 °C (PI400), and (d) 500 °C (PI500).

As the synthetic protocol was successful, a series of PI samples was modified by thermal treatments at 350 °C (PI350), 400 °C (PI400), and 500 °C (PI500) for 15 min. Figure 3 shows the XRD patterns of the PI films treated at different temperatures (the untreated PI film was added for comparison).

Prior to modification, PI shows only a very broad diffraction peak, which is characteristic of an amorphous structure. In contrast, diffraction peaks developed in the range 10–50°, on heating under different conditions. These peaks point to an increasingly ordered structure of the polymer, which results from a higher packing density due to thermally induced chain rearrangement and a decreased free volume owing to the formation of intramolecular and intermolecular bonds in the polymer backbones. The latter are also referred to as charge-transfer complexes (CTC) and ensue in aromatic PI from the interaction between electron donor and acceptor groups fragments of the polymer when these groups approach each other close enough to allow for sufficient electron density exchange [33]. It is important to note that diffraction peaks are already discernible after heating at 350 °C. Moreover, as observed by Inagaki et al. [34], thermal treatment of PI at higher temperatures can lead to the heteroatoms losses, such as oxygen and hydrogen, and also PI chain alignment, forming a plane connected through oxygen bonds. To gain further insight into the chemical evolution and the structure changes of PI films by thermal treatment, TGA, ESR, and XPS measurements were carried out.

The thermal degradation behaviour of the treated PIs was evaluated by TGA under nitrogen atmosphere. Figure 4 presents the TGA curves for the PI films heated at different temperatures.

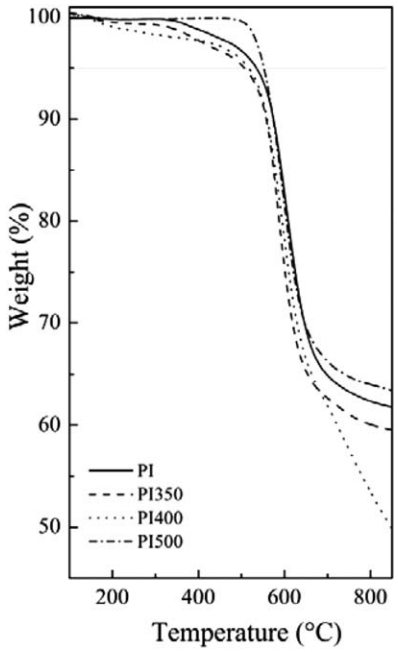

FIG. 4. Thermogravimetric analysis of the synthesized polyimide film before (PI) and after heat treatment at 350 °C (PI350), 400 °C (PI400), and 500 °C (PI500).

The TGA results show changes on the thermal stability of the PI350, PI400, and PI500 samples on heating treatments when compared to the pristine PI sample (prior to thermal treatment). Focusing on the curve profile of the TGA for the both PI350 and PI400 samples, an initial weight loss is observed when the temperature is still below 400 °C, which is the start point of pristine PI thermal degradation. For the PI500 sample instead, no significant changes in TGA curve are observed up to 400 °C. A more detailed understanding of the TGA curves can be gained by analyzing the T_d^5 value of relative weight loss, which indicates the temperature where the sample lost 5% of its weight. For PI T_d^5 was reached at around 538 °C, while for PI350 and PI400 T_d^5 was attained at around 516 °C and 517 °C, respectively. These values revealed a decreasing of the thermal stability of PI350 and PI400, compared to PI. In contrast, the PI500 film started to decompose at higher temperature than the other samples ($T_d^5 = 552$ °C). These results suggest that physical and chemical changes occurred in the PI chain structure during thermal treatment, mainly due to fragment losses. PI500 presumably lost more PI fragments (chemical cleavage) during heating, which results in a higher thermal stability. This suggests that the results observed can be a consequence of polymer chain alignment (thermally induced chain rearrangement), followed by the formation of intramolecular and intermolecular bonds in the polymer backbones at high temperatures. In a recent work, we demonstrated the role played by the time of thermal treatment on the PI decomposition mechanism [35]. We found that not only the amount of products released from PI but also the type of product released is critically influenced by the treatment time. For PI films heated at 500 °C, even for 1 min of thermal treatment, we could observe the release of molecules as a consequence of degradation processes such as homolytical and hydrolytic cleavages, followed by hydrogen ablation, intermolecular coupling, and molecular rearrangements.

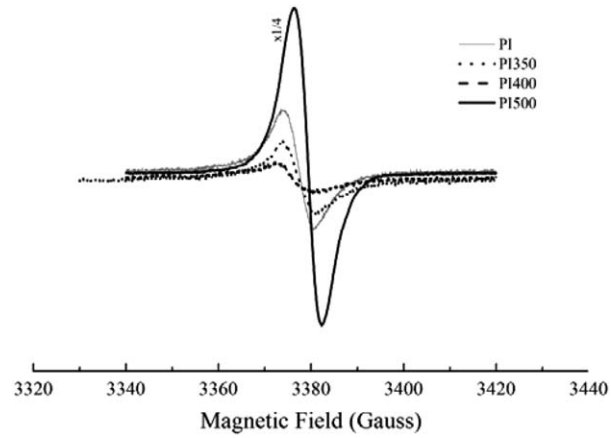

FIG. 5. ESR spectra of the synthesized polyimide film before (PI) and after heat treatment at 350 °C (PI350), 400 °C (PI400), and 500 °C (PI500).

During the initial stage of thermal treatment of PI under inert atmosphere, the polymeric degradation starts with homolytic cleavage of chemical bonds, which leads to free radical formation. This free radical formation can be investigated by ESR spectroscopy, where the signal intensity is proportional to the density of radicals.

Figure 5 presents the ESR spectra of the PI samples before and after thermal treatment. The pristine PI shows a free radical signal assigned to minority homolytic bond cleavage during the imidization process. Interesting, this free radical signal is suppressed in the ESR spectra of the PI350 and 400 samples. As expected, the spectral intensity is higher for PIs treated at higher temperatures (PI500), confirming increased radical formation. The *g*-factor values determined from these spectra were 2.0057 ± 0.0002 for PI, 2.0060 ± 0.0002 for PI350, 2.0063 ± 0.0002 for PI400, and 2.0049 ± 0.0002 for PI500, and the peak-to-peak (ΔH_{pp}) line widths found were 6.3 G for PI, 6.5 G for PI350, 7.5 G for PI400, and 6.2 G for PI500. This ESR characterization is in agreement with a previously reported characterization of Kapton by ESR, where the *g*-factor value for carbonaceous organic free radicals was found to be around 2.0051 and ΔH_{pp} equalled 7.1 G [36]. Differences in *g*-factor value and line width compared to Kapton can be attributed to differences in chemical structure of PI, namely the unpaired electrons delocalized in the aromatic rings containing nitrogen and oxygen and to the unresolved hyperfine interaction of the unpaired electron with the nitrogen nucleus [37]. As the signal intensity is proportional to the density of radicals, it was expected that the ESR signal would scale linearly with the temperature of thermal treatment. Instead one sees that the spectral intensity of the ESR signal decreases for PI350 and PI400 as compared to PI, and then significantly increases for PI500. This unexpected result as well as the variation of ΔH_{pp} and of the *g*-factor value may be an indication that different processes occurred during the formation of these modified PI films. The highest ESR signal for PI500 can be attributed to the increased formation of radicals as a consequence of fragments released by heating. Conversely, the higher peak-to-peak broadening for PI350 (6.5 G) and PI400 (7.5 G) as compared to pristine PI (6.3 G) and PI500 (6.2 G) can be related to the higher dipolar interaction as a consequence of CTC formation or even the formation of new chemical structures. It is important to note that

 DOI 10.1002/pen

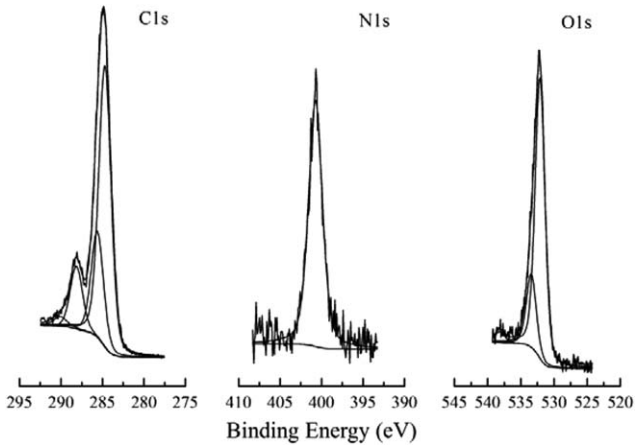

FIG. 6. X-ray photoemission spectra of the C1*s* (left), N1*s* (centre), and O1*s* (right) core level regions of the synthesized polyimide film. Data and fits are shown (for details see text).

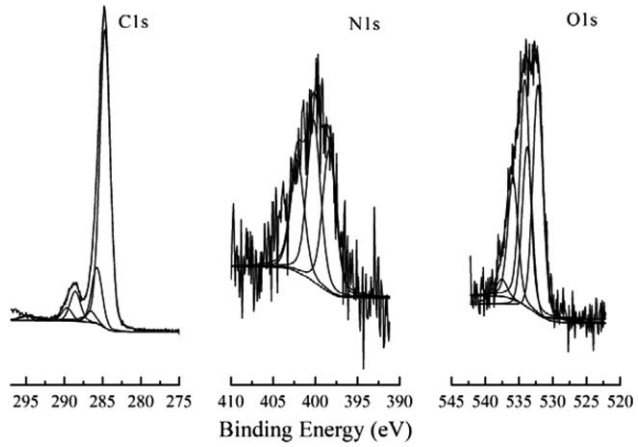

FIG. 7. X-ray photoemission spectra of the C1*s* (left), N1*s* (centre), and O1*s* (right) core level regions of the synthesized polyimide film after heat treatment at 500°C. Data and fits are shown (for details see text).

the peak-to-peak narrowing for the PI500 sample can be explained by the higher conjugation with higher diffusivity of free radicals, thus resulting in less important magnetic dipolar interaction among the spins.

To better understand the role played by these changes after different thermal treatments, XPS spectra were recorded. The XPS spectra of the carbon, nitrogen, and oxygen 1*s* core levels of the pristine PI film are shown in Fig. 6.

In the C1*s* line, the component at 284.7 eV binding energy is attributed to the carbon atoms in benzene rings (C-C and C-H) of the BTDA structure; the component at 285.6 eV derives from carbon atoms bound to nitrogen, while the component at 288.1 eV corresponds to C═O double bonds. The N1*s* peak shows a symmetric line centred at 400.7 eV binding energy assigned to nitrogen in the PI by similarity to uracil base [38], while the O1*s* peak is asymmetric and was fitted to two components. The O1*s* components at 532.1 and 533.4 eV are attributed to C═O bonds in the imide ring and C═O from ketone of the PI structure [29]. The peak at 290.1 eV in C1*s* and 538.1 eV in O1*s* spectra are so-called shake-up satellite structures associated with π to π^* transitions; their intensity amounts to around 5% of the C—C and C═O peak areas, respectively. The spectral assignments of the pristine PI sample in this work agree with previously reported results [39].

The ratios of the peak intensities and the corresponding surface composition, calculated from the integral intensities of the component peaks of PI film taking into account the sensitivity factors for each element specific to the spectrometer used, are shown in Table 1.

The experimental atomic ratios obtained for the pristine PI film are in relatively good agreement with the corresponding theoretical values calculated from the empirical formula. Treatment at 500 °C results in significant changes in the peak shapes and positions, as shown in Fig. 7. In the C1*s* spectrum the component at 284.7 eV, related to C—C and C—H bonds, markedly increased whereas the components at 285.7 and 288.6 eV, which correspond to C—N and C═O bonds, respectively, decreased. Such increase in the 284.7 eV peak intensity (area) is in agreement with the ESR peak-to-peak broadening and increase in the C/O ratio, thus reinforcing the hypothesis of thermally induced formation of a graphite-like structure on the PI surface. New components at 286.6 and 289.4 eV appeared. The latter component is shifted in binding energy by 1.5 eV with respect to the C═O spectral signature of the pristine film (Fig. 6), which indicates that the carbonyl group is a non-imide carbonyl [40]. These peaks are located at binding energies corresponding to bonds present in nitrile, ether or ester groups, according to the literature [39–41]. In addition, the nitrogen 1*s* peak is no longer symmetric, which suggests that a substantial percentage of the imide rings broke during thermal treatment, releasing small oxygen- and nitrogen-containing moieties. The component at 400.2 eV binding energy in the N1*s* spectrum is due to the imide C═N bond, and the new ones at 398.3 eV (related to amine) and 402.1 eV are probably associated with alkylammonium bonds [42] formed during sample heating. These results show no evidence of amide or nitrile formation. In the O1*s* core level region, four components are detected at 532.2, 533.8, 534.7, and 536.3 eV binding energy; the first and the second one arise from the carbonyl groups (C═O) in the imide system, the third and the fourth component may be related to C—O bonds present in the ester groups. In general, literature reports binding energies around 533.0 eV for ester functional groups [43] and the difference found in this study may be a consequence of the overlapping bands of amines oxides and ester groups, which give rise to peak broadening and as well as binding energy shifts. The binding energies of all C1*s* components identified for PI and PI500 are listed in Table 2. By comparing to the pristine PI film in Table 1, the increase of both the C/O and C/N atomic ratios are an indication of graphite-like structures on the outmost surface layer of the thermally treated PI500, in agreement with their larger peak-to-peak distance in the ESR lines, confirming a

TABLE 1. Surface composition and ratios between different elements before and after thermal treatment at 500°C of the polyimide membranes as measured by XPS and theoretical value for pristine PI.

Sample	C (%)	O (%)	N (%)	C/O	C/N
Theoretical value	76.6	16.7	6.7	4.6	11.4
PI	75.8 ± 0.4	17.0 ± 0.2	7.3 ± 0.6	4.5 ± 0.5	10.4 ± 0.9
PI500	84.4 ± 0.2	10.2 ± 0.2	5.3 ± 0.5	8.3 ± 1.5	17.1 ± 1.3

TABLE 2. Binding energy and relative contribution to the C1*s* peak area obtained by conventional XPS analysis.

	C-C C-H		-N-C=O		C-N		C=O		C=O[a]		Shake up	
Sample	Peak (eV)	Area (%)	Peak (eV)	Area (%)	Peak (eV)	Area (%)	Peak (eV)	Area (%)	Peak (eV)	Area (%)	Peak (eV)	Area (%)
PI	284.7	61	285.6	23	—	—	288.1	13	—	—	290.1	4
PI500	284.7	71	285.7	13	286.6	3	288.6	7	288.6	3	295.3	3

[a]C = O non-imidic.

chemical evolution by loss of moieties containing oxygen and nitrogen to form these graphite-like structures.

To investigate also the effect of the thermal treatments on the sub-surface layers of the films, photoemission experiments with photon energy of 4,000 eV were carried out. At this excitation energy, the analysis depth is about 10–20 nm, which is deeper than the surface layer accessible using a Al Kα ($h\nu = 1{,}486.6$ eV) laboratory source [44]. The C1*s* spectra acquired with synchrotron radiation of PI films before and after thermal treatments are shown in Fig. 8.

The C1*s* spectrum for pristine PI (Fig. 8a) showed components at 283.8 and 284.7 eV related to C—H and C—C bonds, a spectral contribution at 285.0 eV, which stems from C—N bonds, and a component at 287.9 eV that can be assigned to carbonyl bonds. The peak at higher binding energy is a shake-up feature. The N1*s* spectrum of PI presented two components, the main one at 400.1 eV, related to C-N imide bonds, and one at lower binding energy (398.8 eV), which can be assigned to NH_2 group present in the end of PI chain and represents around 4% of the total peak area. In the O1*s* core level region, components at 531.5, 532.8, and 537.3 eV binding energy were detected. The lower binding energy component is related to imide carbonyl groups, the second component corresponds to C═O bonds from PI chemical structure [43] and the component at higher binding energy is the shake-up feature. After thermal treatment at 350 °C, the XPS photoemission spectra of PI350 shows the same components as for the pristine film before heating (Fig. 8b). Conversely, PI thermally treated at 400 °C

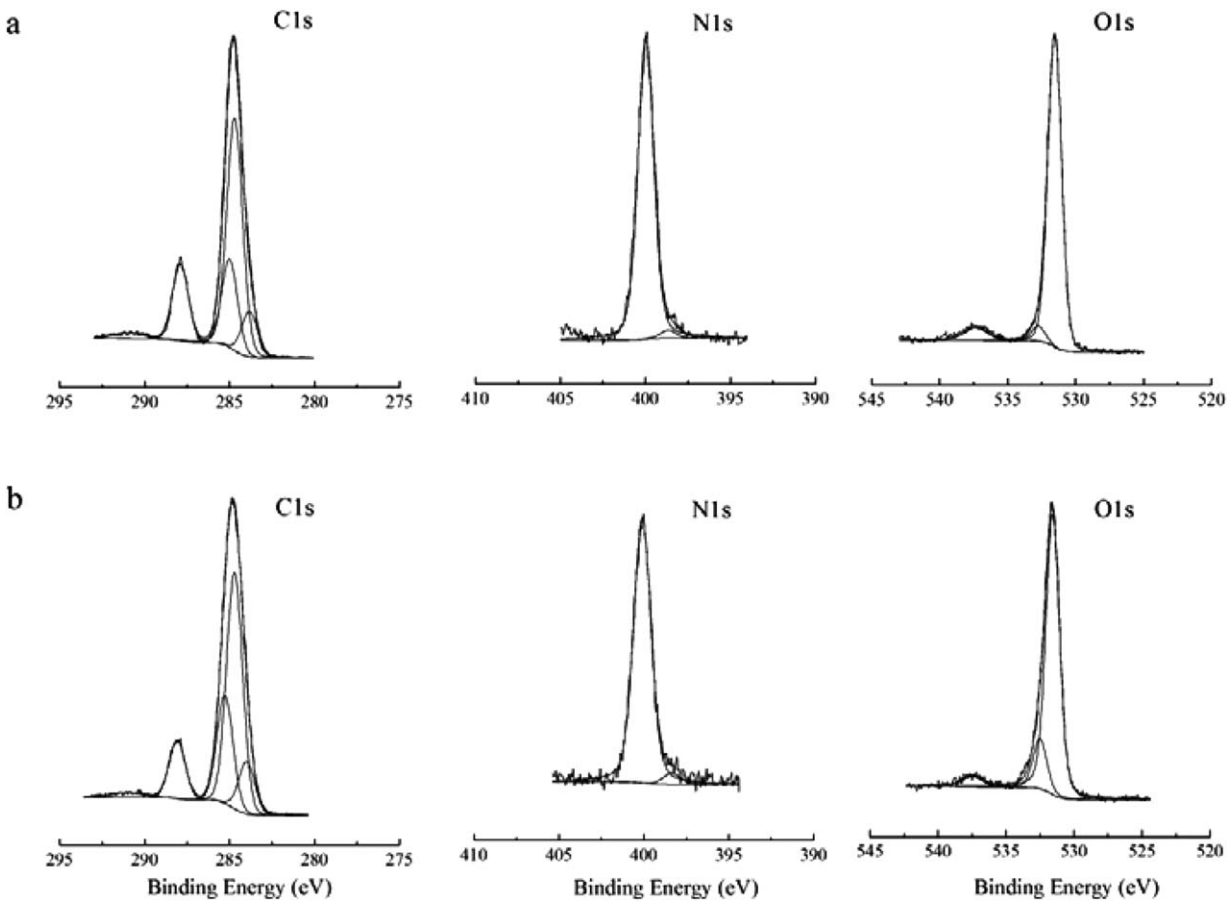

FIG. 8. Photoemission spectra ($h\nu = 4{,}000$ eV) of the C1*s* (left), N1*s* (centre) and O1*s* (right) core level regions of the synthesized PI film (a) before and (b) after heat treatment at 350 °C (PI350). Data and fits are shown (for details see text).

 DOI 10.1002/pen

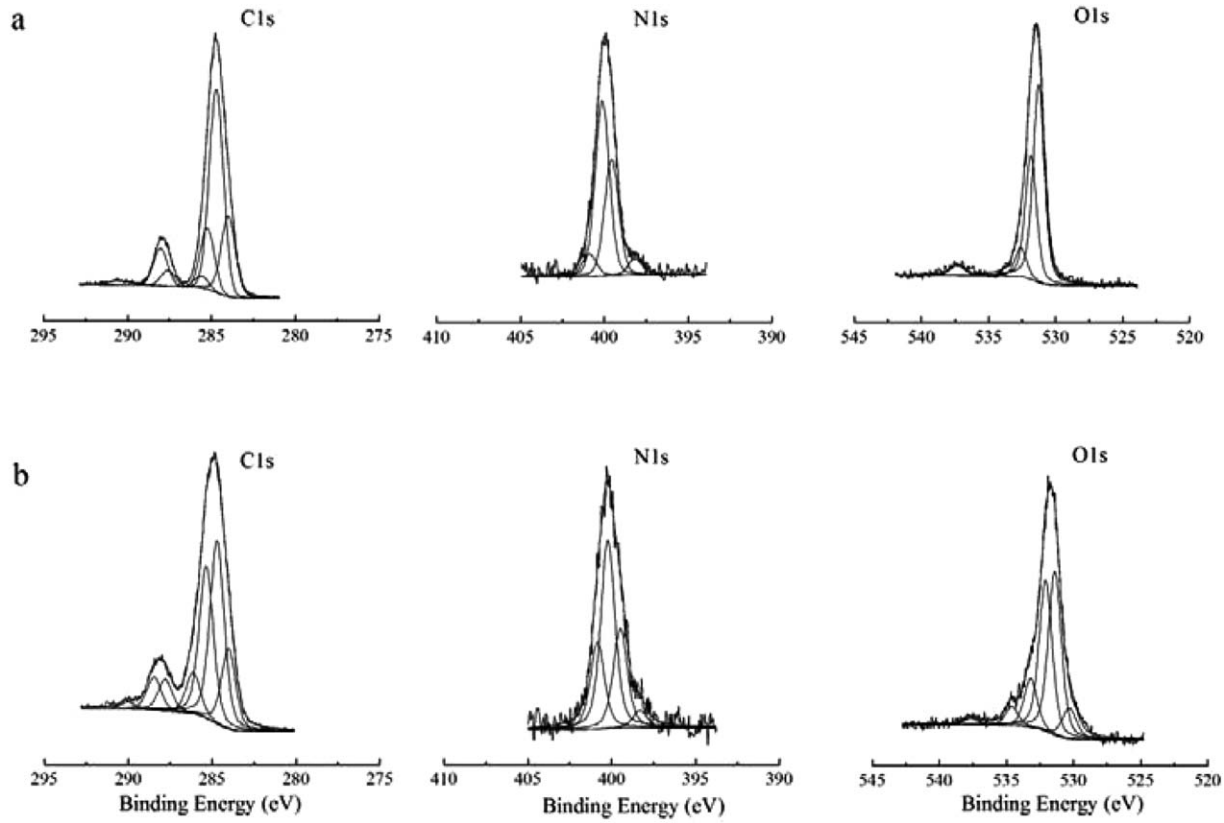

FIG. 9. Photoemission spectra ($h\nu = 4{,}000$ eV) of the C1*s* (left), N1*s* (centre) and O1*s* (right) core level regions of PI films after heat treatment (a) at 400 °C (PI400) and (b) 500 °C (PI500). Data and fits are shown (for details see text).

(PI400) presents pronounced changes in the C1*s*, N1*s*, and O1*s* spectra as compared to PI. In the C1*s* photoemission spectrum of PI400 (Fig. 9a), new components assigned to amide or nitrile groups (285.7 eV) and ester (287.6 eV) were detected. In the N1*s* core line, a new component at 399.6 eV is detected. This component can be related to nitrile [45] or amide [46] compounds. However, as the C1*s* for C—N component for nitrile groups appears at 286.7 eV [45], the components at 285.7 eV in the C1*s* spectrum and at 399.6 eV in the N1*s* spectrum are assigned as amide compounds. In addition, a primary alkyl ammonium component (C-NH_3^+) at 400.9 eV is also found [42]. The O1*s* core level region shows components at 531.3, 531.9, 532.7, and 537.4 eV binding energy, which correspond to imide C═O bonds (the first and the second components), amide bonds and shake-up features. It is important to note that the area of the component at 531.9 eV (related to the ketone from PI chain) increased with the increase with treatment temperature, which suggests the contribution of amide formation as this binding energy is characteristic of carbonyl in amide compounds [46]. For PI500 films, the C1*s* and N1*s* spectra showed the components already identified for PI400 (Fig. 9b) but the O1*s* spectrum presented two new contributions at 529.9 eV, assigned to O—H bonds [47], and 534.6 eV related to ester groups [41–43], confirming the formation of ester bonds at higher temperature of thermal treatment. Analogously to the signature of pyrolysis in the C1*s*, the peak area of the imidic component in the N1*s* line decreased from 97% of the total N1*s* intensity of the pristine PI film to 48% for PI500. For this sample in the O1*s* spectrum, the imidic component also showed an intensity decrease as compared to PI350 or PI400, while the non-imidic component increased after thermal treatments, from 4% of the total O1*s* intensity in the PI film treated at 350 °C (PI350) to 11% (PI500).

The atomic ratio of C/N was 12.5 ± 3 for PI, 9.0 ± 4 for PI350, 8.0 ± 4 for PI400, and 8.9 ± 2, for PI500, while the C/O atomic ratio amounted to 4.6 ± 1.5 for PI, 4.1 ± 0.5 for PI350, 4.2 ± 0.4 for PI400, and 3.8 ± 0.3 for PI500. Both atomic ratios show the release of O- and N-containing moieties during thermal treatment. Using TG/MS analysis Xie et al. [48] demonstrated that–C_6H_3-NH_2/-C_6H_4-NH- groups are released at 420 °C and that the release of C_6H_3-CO- occurs at 500 °C. Our findings are in agreement with these results.

Thermal treatments of PI films have been studied for decades and different mechanism of PI decomposition, which can take place depending on the PI chemical structure and thermal treatment conditions, have been proposed [16, 49–51]. Carbon-nitrogen and carbon-oxygen are the first bonds to be cleaved, leading to a carbon-rich PI material. From the above results, it can be observed that thermal treatment at 350 °C promoted no significant changes in the PI chemical structure; it gave rise only to the rearrangement of polymer chains and increased the degree of crystallinity, as confirmed by XRD. Only after thermal treatment at 400 °C peaks related to amine, nitrile, and oxygen-bonded groups started to appear in the photoemission

spectra, indicating imidic bond cleavage through homolytic fragmentation as supported by ESR. Heating the polymer at 500 °C led to ester bond formation, which implies release of more moieties, polymer chain rearrangement and chain-chain interactions. However, due to the short heating time used in this work, part of the PI film remains mostly unchanged, as evidenced by the presence of the shakeup feature even after thermal treatment at 500 °C. In a recent work, Xu and Wang [52] also observed structural changes in PIs membranes by heating at temperature in the range 250 °C to 400 °C. These authors showed that denser membrane morphology or crosslinking among polymer chains can be obtained as a consequence of the thermal treatment.

In summary, the results obtained showed that mild thermal treatment conditions promoted different structural and chemical changes in the PI films. The release of nitrogen and oxygen species, a decrease of interchain space, the formation of a large population of free radicals as well as the formation of different chemical bonds can be obtained while maintaining most of the PI chemical structure intact. XPS analysis showed that the chemical structure changes not only on the outer surface but also in the polymer chain layers below. These modifications can promote the reduction of the free volume in the polymer structure, increasing the rigidity of the polymer chains and consequently promote changes in properties such as pervaporation [53] of a PI membrane.

CONCLUSIONS

Thermal treatment of PI films at mild temperatures (350 °C and 400 °C) and at a temperature close to polymer degradation temperature (500 °C) for short times (15 min) was investigated. Heating at 350 °C was found to promote polymer chain motion leading to a well-ordered polymer chain. This chain stacking probably allows for chain-chain interaction, which stabilizes the radicals formed during thermal treatment at higher temperatures. Further temperature increase to 500 °C increases the free radical population. By following the changes in chemical structure of the PI films after each heat treatment by XPS analysis, we discovered that the thermal treatment protocol chosen gave rise to new chemical bonds, such as amide and ester, while preserving most of the initial polymer chain structure intact. This controlled thermal treatment strategy opens up the possibility to create materials with tuned characteristics in a step-by-step fashion.

ACKNOWLEDGMENTS

Experiments at the Laboratory of Synchrotron Light Helmholtz-Zentrum Berlin für Energie und Materialien HZB Bessy II, Berlin were supported by the Transnational Access-programme within the European Commission's Integrated Infrastructure Initiative (I3) "Coordinated Access to Light sources to promote Standards and Optimization" (CALIPSO). We also thank José Fernando de Lima and Professor Dr. Claudio José Magon (Institute of Physics of São Carlos, University of São Paulo, Brazil) for EPR analysis.

REFERENCES

1. C.E. Sroog, *Prog. Polym. Sci.*, **16**, 561 (1991). doi:10.1016/0079-0000(91)90010-I.
2. D.J. Liaw, K.L. Wang, Y.C. Huang, K.R. Lee, J.Y. Lai, and C.S. Ha, *Prog. Polym. Sci.*, **37**, 907 (2012). doi:10.1016/j.progpolymsci.2012.02.005.
3. J.K. Fink, "Poly(imide)s," in *High Performance Polymers - A Volume in Plastics Design Library*, 2nd ed., Elsevier Inc., Oxford, 475 (2008). doi:10.1016/B978-0000-0000.50001-0000.
4. Y. Guan, C. Wang, D. Wang, G. Dang, C. Chen, H. Zhou, and X. Zhao. *Polymer (Guildf)*, **62**, 1 (2015). doi:10.1016/j.polymer.2015.02.009.
5. H.B. Park, C.H. Jung, Y.M. Lee, A.J. Hill, S.J. Pas, S.T. Mudie, E.V. Wagner, B.D. Freeman, and D.J. Cookson. *Science*, **318**, 254 (2007). doi:10.1126/science.1146744.
6. R. Shindo, N. Yamanaka, T. Wakamatsu, and K. Nagai, *Polym. Eng. Sci.*, **56**, 178 (2016). doi:10.1002/pen.24241.
7. S. Yoo, Y.H. Kim, J.W. Ka, Y.S. Kim, M.H. Yi, and K.S. Jang, *Org. Electron. Phys, Mater. Appl.*, **23**, 213 (2015). doi:10.1016/j.orgel.2015.05.012.
8. H. Pan, S. Chen, Y. Zhang, M. Jin, Z. Chang, and H. Pu, *J. Membr. Sci.*, **476**, 87 (2015). doi:10.1016/j.memsci.2014.11.023.
9. L. Akbarian-feizi, S. Mehdipour-ataei, and H. Yeganeh, *Int. J. Hydrogen Energy*, **35**, 9385 (2010). doi:10.1016/j.ijhydene.2010.03.072.
10. W. Li, X. Guo, and J. Fang, *J. Mater. Sci.*, **49**, 2745 (2014). doi:10.1007/s10853-0000-0000-0000.
11. G.A. Niklasson and I.A. Serbinov, *J. Mater. Sci.*, **23**, 2601 (1988). doi:10.1007/BF01111921.
12. R.J. Swaidan, X. Ma, E. Litwiller, and I. Pinnau, *J. Membr. Sci.*, **495**, 235 (2015). doi:10.1016/j.memsci.2015.08.015.
13. R. Swaidan, B. Ghanem, E. Litwiller, and I. Pinnau, *J. Membr. Sci.*, **475**, 571 (2015). doi:10.1016/j.memsci.2014.10.046.
14. Y. Xiao, B.T. Low, S.S. Hosseini, T.S. Chung, and D.R. Paul, *Prog. Polym. Sci.*, **34**, 561 (2009). doi:10.1016/j.progpolymsci.2008.12.004.
15. S. Kanehashi, M. Onda, R. Shindo, S. Sato, S. Kazama, and K. Nagai, *Polym. Eng. Sci.*, **53**, 1667 (2013). doi:10.1002/pen.23425.
16. P.S. Tin, Y. Xiao, and T. Chung, *Purif. Rev.*, **35**, 285 (2006). doi:10.1080/15422110601003481.
17. H. Kawakami, M. Mikawa, and S. Nagaoka, *J. Membr. Sci.*, **118**, 223 (1996). doi:10.1016/0376-0000(96)00115-0000.
18. A.B. Fuertes, D.M. Nevskaia, and T.A. Centeno, *Microporous Mesoporous Mater.*, **33**, 115 (1999). doi:10.1016/S1387-0000(99)00129-0000.
19. M. Iwase, A. Sannomiya, S. Nagaoka, Y. Suzuki, M. Iwaki, and H. Kawakami, *Macromolecules*, **37**, 6892 (2004). doi:10.1021/ma040077y.
20. A. Bos, I.G.M. Pünt, M. Wessling, and H. Strathmann, *Sep. Purif. Technol.*, **14**, 27 (1998). doi:10.1016/S1383-0000(98)00057-0000.
21. K.M. Steel and W.J. Koros, *Carbon N. Y.*, **41**, 253 (2003). doi:10.1016/S0008-0000(02)00309-0000.
22. X. Chen, L. Hong, X. Chen, W.H.A. Yeong, and W.K.I. Chan, *J. Membr. Sci.*, **379**, 353 (2011). doi:10.1016/j.memsci.2011.06.007.
23. C.J. Anderson, S.J. Pas, G. Arora, S.E. Kentish, A.J. Hill, S.I. Sandler, and G.W. Stevens, *J. Membr. Sci.*, **322**, 19 (2008). doi:10.1016/j.memsci.2008.04.064.

24. A. Ismail and L. David, *J. Membr. Sci.*, **193**, 1 (2001). doi: 10.1016/S0376-0000(01)00510-0000.
25. W. Volksen, "Polyimides: Polymerization and Properties," in *Encyclopedia of Materials: Science and Technology*, Elsevier Science Ltd, 7189, Oxford (2001).
26. S.H. Hsiao and Y.-J.J. Chen, *Eur. Polym. J.*, **38**, 815 (2002). doi:10.1016/S0014-0000(01)00229-0000.
27. M. Gorgoi, S. Svensson, F. Schäfers, G. Öhrwall, M. Mertin, P. Bressler, O. Karis, H. Siegbahn, A. Sandell, H. Rensmo, W. Doherty, C. Jung, W. Braun, W. Eberhardt. *Nucl. Instruments Methods Phys. Res. Sect. A Accel. Spectrometers, Detect. Assoc. Equip.*, **601**, 48 (2009). doi:10.1016/j.nima.2008.12.244.
28. J.F. Moulder, W.F. Strickle, P.E. Sobol, and K.D. Bomben, *Handbook of X-ray Photoelectron Spectroscopy: A Reference Book of Standard Spectra for Identification and Interpretation of XPS Data*, Physical Electronics Eden Prairie, MN, Minnesota (1992).
29. O. Ivashenko, J.T. Van Herpt, B.L. Feringa, W.R. Browne, and P. Rudolf, *Chem. Phys. Lett.*, **559**, 76 (2013). doi:10.1016/j.cplett.2012.12.060.
30. J.N. Barsema, S.D. Klijnstra, J.H. Balster, NF.A. van der Vegt, G.H. Koops, and M. Wessling, *J. Membr. Sci.*, **238**, 93 (2004). doi:10.1016/j.memsci.2004.03.024.
31. W.S. Li, Z.X. Shen, J.Z. Zheng, and S.H. Tang, *Appl. Spectrosc.*, **52**, 985 (1998). doi:10.1366/0003702981944625.
32. I. Sava, Ş. Chişcă, M. Brumă, and G. Lisa, *J. Therm. Anal. Calorim.*, **104**, 1135 (2011). doi:10.1007/s10973-0000-0000-0000.
33. K. Vanherck, G. Koeckelberghs, and I.F.J. Vankelecom, *Prog. Polym. Sci.*, **38**, 874 (2013). doi:10.1016/j.progpolymsci.2012.11.001.
34. M. Inagaki, S. Harada, T. Sato, T. Nakajima, Y. Horino, and K. Morita, *Carbon N. Y.*, **27**, 253 (1989). doi:0008-0000/89.
35. F.A.S. Ferreira, L.C. Battirola, J.P. Lewicki, M.A. Worsley, M.A. Pereira-da-Silva, T. Amaral, C.M. Lepienski, and U.P. Rodrigues-Filho, *Polym. Degrad. Stab.*, **129**, 399 (2016). doi: https://doi.org/10.1016/j.polymdegradstab.2016.05.001.
36. K. Rasmussen, G. Grampp, M. van Eesbeek, and T. Rohr, "Thermal and UV Degradation of Polyimides and Silicones Studied in situ with ESR Spectroscopy," in Proceedings of 11th International Syposium on Materials in a Space Environment (2009).
37. M.A. George, B.L. Ramakrishna and W.S. Glaunsinger, *J. Phys. Chem.*, **94**, 5159 (1990).
38. J. Peeling, F.E. Hruska, D.M. McKinnon, M.S. Chauhan, and N.S. McIntyre, *Can. J. Chem.*, **56**, 2405 (1978). doi:10.1139/v78-0000.
39. A.M.U. Ektessabi and S. Hakamata, *Thin Solid Films*, **377–378**, 621 (2000). doi:10.1016/S0040-0000(00)01444-0000.
40. K. Yung, D. Zeng, and T. Yue, *Surf. Coat. Technol.*, **160**, 1 (2002). doi:10.1016/S0257-0000(02)00384-0000.
41. D.T. Clark and H.R. Thomas, *J. Polym. Sci. Polym. Chem. Ed.*, **16**, 791 (1978). doi:10.1002/pol.1978.170160407.
42. F. Pippig, S. Sarghini, A. Holländer, S. Paulussen, and H. Terrvn, *Surf. Interface Anal.*, **41**, 421 (2009). doi:10.1002/sia.3043.
43. G.P. López, D.G. Castner, and B.D. Ratner, *Surf. Interface Anal.*, **17**, 267 (1991). doi:10.2307/302397.
44. J.C. Vickerman and I.S. Gilmore, *Surface Analysis: The Principal Techniques*, 2nd ed., Wiley Online Library, Chichester (2009).
45. F. Le Normand, J. Hommet, T. Szörényi, C. Fuchs, and E. Fogarassy, *Phys. Rev. B*, **64**, 235416 (2001). doi:10.1103/PhysRevB.64.235416.
46. J. Charlier, V. Detalle, F. Valin, C. Bureau, and G. Le, *J. Vac. Sci. Technol. A*, **15**, 353 (1997). doi:10.1116/1.580491.
47. B.J. Tan, K.J. Klabunde, and P.M.A. Sherwood, *J. Am. Chem. Soc.*, **113**, 855 (1991).
48. W. Xie, R. Heltsley, X. Cai, F. Deng, J. Liu, C. Lee, and W-P. Pan, *J. Appl. Polym. Sci.* **83**, 1219–1227 (2002).
49. Y. Kim, H. Park, and Y. Lee, *J. Membr. Sci.*, **255**, 265 (2005). doi:10.1016/j.memsci.2005.02.002.
50. K. Yung, D. Zeng, and T. Yue, *Appl. Surf. Sci.*, **173**, 193 (2001). doi:10.1016/S0169-0000(00)00884-0000.
51. V.E. Smirnova, I.V. Gofman, T.A. Maritcheva, V.E. Yudin, K. Eto, T. Takeichi, Y. Kaburagi, and Y. Hishiyama, *Carbon N. Y.*, **45**, 839 (2007). doi:https://doi.org/10.1016/j.carbon.2006.11.012.
52. S. Xu and Y. Wang, *J. Membr. Sci.*, **496**, 142 (2015). doi: 10.1016/j.memsci.2015.08.055.
53. F. Zhou and W.J. Koros, *Polymer (Guildf)*, **47**, 280 (2006). doi: https://doi.org/10.1016/j.polymer.2005.11.017.